Sensors and Materials, Vol. 10, No. 7 (1998) 413–424
MYU Tokyo

S & M 0343

Dynamic Modeling of a Tunable Microgyroscope

Myung-Seok Kang, Sung-Kie Youn*, Young-Ho Cho and Ki Bang Lee

Department of Mechanical Engineering, Korea Advanced Institute of Science and Technology
373-1, Kusung, Yusung, Taejon, 305-701, Korea

(Received March 18, 1997; accepted December 9, 1997)

Key words: tunable microgyroscope, electrostatic combs, Coriolis force, frequency matching, stiffness, damping

The modeling of an electrostatically tunable microgyroscope is presented. The main structure of the microgyroscope developed consists of two micro-suspended plates driven by electrostatic combs in the antisymmetric tuning-fork mode. The natural frequency of the plates in the direction normal to the comb driving direction is tunable to match the frequencies of the gyroscope. Modeling and derivation of the dynamic properties of the model are discussed. The issues in this process are those commonly associated with the modeling and simulation of MEMS devices.

1. Introduction

Considerable work has been carried out on developing surface-micromachined resonant microgyroscopes.[1,2] Surface-machined microgyroscopes have attractive features such as low manufacturing cost, small size, relatively high performance and low power consumption. The drawback is their dimensional inaccuracy compared with the device size due to micromachining errors inherent in the etching processes. Therefore the natural frequencies of such devices tend to drift away from designed values. Attempts have been made to come up with designs in which the effective stiffness of the device structure is modified using fringing-field forces.[3,4]

In the microgyroscope described herein, the effective stiffness, and thus the natural frequency is tuned by electrostatic forces between two parallel plates. To design the device, a simple and effective model of the microgyroscope is developed. The structure of the microgyroscope has several distinctive features. The calculation of the stiffnesses and dampings of the gyroscope structure is discussed in detail.

*To whom correspondence should be directed.

2. The Tunable Microgyroscope

The features of the microgyroscope are as follows:

a. It has a surface micro-machined poly-Si structure.

b. It is driven by electrostatic combs.

c. It detects changes in capacitance due to an induced Coriolis force.

d. The natural frequency of the out-of-plane motion of the plate is tunable.

Figure 1 shows the schematic diagram of the microgyroscope. The two plates are driven in the antisymmetric tuning-fork mode by electrostatic combs. When the input angular rate Ω is imposed on the device and the plates are excited, Coriolis forces are developed that push the plates in opposite directions toward or away from the substrate electrodes. These motions change the capacitances in the gaps between the plates and the bottom electrodes on the substrates.

The term V_D in the diagram is the comb drive voltage. The effective stiffness of the structure in the z-direction can be adjusted by the voltage V_c, which is applied between the plate and the bottom electrode and develops an electrostatic force pulling the plate toward the bottom electrode. The large holes in the plates reduce the inertia and improve the release etch of the sacrificial layer. Figure 2 shows a SEM picture of the manufactured microgyroscope.

3. Mechanical Model of the Microgyroscope

Only half of the structure of the microgyroscope is modeled since both halves are symmetrical. Figure 3 shows a simple mechanical model of the structure assuming that the plate oscillates only in a translational mode.

Because the plate is much stiffer compared to other parts of the structure, it is modeled as a rigid mass. The stiffnesses and dampings of the structure are modeled by the dampers

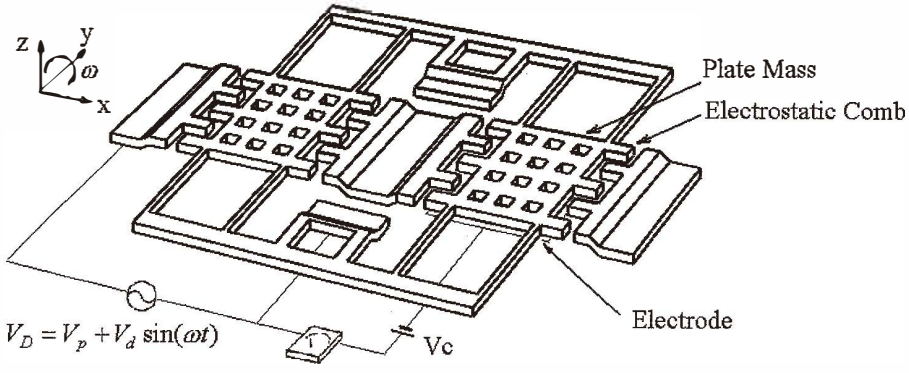

Fig. 1. Schematic diagram.

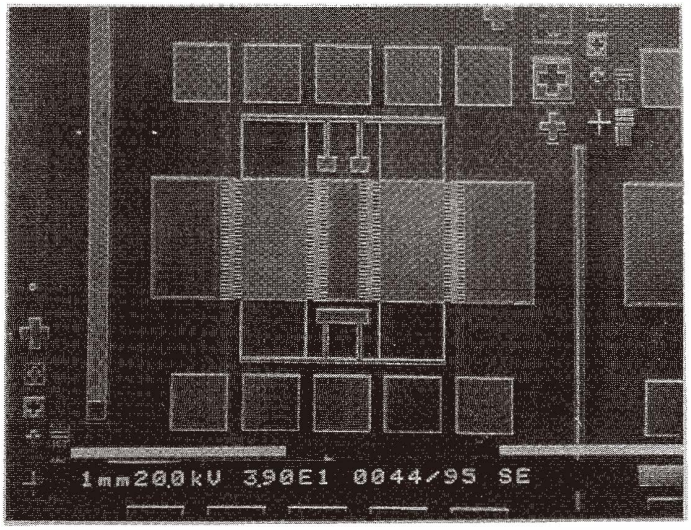

Fig. 2. SEM picture of the manufactured microgyroscope.

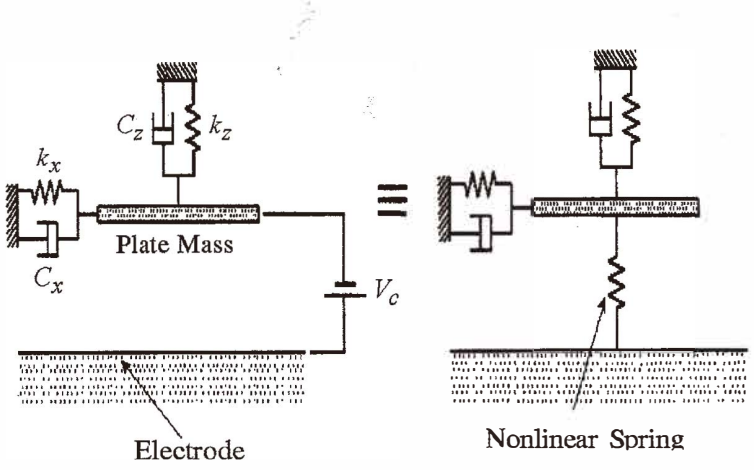

Fig. 3. Mechanical model of the microgyroscope.

and springs in the x- and z-directions. The electrostatic force developed by the voltage V_C applied between the plate and the bottom electrode is modeled by a nonlinear spring.

The presence of the nonlinear spring changes the stiffness of the structure in the z-direction. When the initial gap d_0 between the plate and the electrode is reduced to d due to the Coriolis force induced by the external angular velocity in addition to the applied

electrostatic force, the force developed in the mechanical spring becomes $f_{z,spring} = k_z(d_0 - d)$. Then the electrostatic force or the force developed in the nonlinear spring becomes $f_{z,spring} = -\frac{1}{2}\varepsilon A V_C^2 / d^2$. A is the area of the plate surface facing the electrode on the substrate, and ε is the permeability.

Static equilibrium is achieved when the magnitudes of the two spring forces are the same. In the absence of the Coriolis force, the spring constant $k_{z,elect}$ of the electrostatic force at the equilibrium position is defined by the equilibrium condition as $k_{z,elect} = 2k_{z,spring}(d_0/d_{eq} - 1)$ Small amplitudes of oscillations are considered. We obtain the effective stiffnesses of the nonlinear spring in the z-direction as

$$f_{z,effect} = f_{z,elect}\Big|_{d=d_{eq}} + k_{z,elect}(d - d_{eq}) \,. \tag{1}$$

Therefore, the effective stiffness in the z-direction becomes

$$\begin{aligned} f_{z,effect} &= k_{z,spring} - k_{z,elect} \\ &= k_{z,spring}(3 - 2\frac{d_0}{d_{eq}}) \,. \end{aligned} \tag{2}$$

The control voltage can also be determined from the equilibrium relation

$$f_{z,spring}(d_0 - d_{eq}) = \frac{1}{2}\varepsilon A \frac{V_C^2}{d_{eq}^2}$$

as

$$V_C = \sqrt{\frac{2}{\varepsilon A} k_{z,spring} d_{eq}^2 (d_0 - d_{eq})} \,. \tag{3}$$

Due to the change in the effective stiffness in the z-direction, the natural frequency in the direction also changes to

$$\omega_{z,effect} = \omega_{z,spring}\sqrt{3 - 2\frac{d_0}{d_{eq}}} \,, \tag{4}$$

where $\omega_{z,spring}$ is the natural frequency of the structure in the z-direction in the absence of the applied electrostatic force.

4. The Equations of the Motion

The equations of motion of the plate in the x- and z-directions are, respectively,

$$m_x\ddot{x} + c_x\dot{x} + k_x x = f_0 \sin \omega t \tag{5a}$$

$$m_z\ddot{z} + c_z\dot{z} + k_z z = f_C. \tag{5b}$$

The effective mass of the plate in the z-direction is slightly larger than that in the x-direction.

In the preceding equations, f_0 is the magnitude of the electrostatic force developed in the comb due to the comb drive voltage $V_D = V_d + V_p \sin \omega t$ and can be expressed as

$$f_0 = \frac{\partial C_D}{\partial x} V_p V_d, \tag{6}$$

where C_D is the total capacitance of the comb. Also f_C, the Coriolis force induced on the plate due to the external input rotational velocity Ω of the structure, is expressed as

$$f_C = -2m\Omega\dot{z}. \tag{7}$$

The plate is driven by the electrostatic force developed in the comb, and the motion in the x-direction can be determined when it is used in eq. (5a). The plate is driven in the z-direction by the Coriolis force, which can be determined from Ω and the solution x from eq. (5a). It is modeled as eq. (5b), the solution of which is

$$z = -2\Omega \frac{\omega}{\omega_{z,effect}^2} \frac{f_0}{k_x} R_x R_z \cos(\omega t - \phi_x - \phi_z), \tag{8}$$

where R_x and R_z are the magnification factors in the x- and z-directions respectively, ϕ_x and ϕ_z the phase lags due to structural dampings in the corresponding directions, and ω_{nz} is the natural angular velocity. When the natural frequencies in the x- and z-directions are the same, the magnitude of z is maximized.

Once the solution is known, the sensitivity of the capacitance in the microgyroscope can be calculated using the following relations:

$$\frac{\Delta C}{\Omega} = \frac{\Delta z}{\Omega} \frac{\partial C}{\partial z}\Big|_{z=d_{eq}} \tag{9a}$$

and

$$\Delta C = \Delta z \frac{\partial C}{\partial z}\Big|_{z=d_{eq}}. \tag{9b}$$

5. Calculation of Structural Properties

The calculation of the stiffnesses of the structure in the x- and z-directions can be carried out in a straightforward manner. The stiffness in the x-direction k_x can be determined by considering the four arms supporting the plate as Euler beams as shown in Fig. 4. As presented in Fig. 4, the four arms that connect the plate to the side support beams are very flexible compared to other parts. Therefore, they can be assumed to act as Euler beams while the other parts are assumed to be rigid. For the calculation of the effective stiffness in the z-direction, we need to know the pure structural stiffness. The behavior of the device in the z-direction illustrated in Fig. 5 is not as simple as the case in the x-direction.

The whole structure is modeled with finite elements and the stiffness is calculated using the finite element model. The effective stiffness can be obtained from eq. (2).

The most difficult part of the analysis is to calculate the damping coefficients. In the calculation of damping coefficients, air is assumed to be a viscous fluid. The in-plane damping, or the damping in the x-direction, is expressed as follows when a uniform velocity gradient in the gap between the plate and the bottom electrode is assumed:

$$c_x = \mu \frac{A}{h}, \tag{10}$$

where μ is the viscosity of the air, h is the gap size, and A is the surface area of the plate.

Of course, this model may be too simple to represent the actual situation. When the small oscillations are involved, it could give reasonable results. Otherwise the velocity field of the surrounding fluid must be computed from the Navier-Stokes equation to calculate the viscous drag damping force. However, for a low viscosity fluid like air, slipping occurs and the normal component of the velocity vanishes on the surface.

For the calculation of the out-of-plane damping or damping in the z-direction, a squeeze film model is adopted. Figure 6 depicts a plate with holes. As the plate moves in the direction normal to the plane, the air between the plate and the bottom electrode is squeezed and flows out through the holes. When the fluid inertia and dilatational stresses are neglected and small Reynolds number is assumed, the generalized Reynolds equation becomes

$$\nabla^2 p = 12 \frac{\mu}{h^3} \dot{h}, \tag{11}$$

where p is the gage pressure of the air in the gap.

Having large holes in the plate provides a big advantage, for when there are no such holes, the air must escape the gap through the sides of the plate. As the frequency of the motion of the plate increase, the air trapped in the gap does not have enough time to respond and thus acts like a spring. The big holes prevent the air from acting like spring and at the same time allow excellent release etch of the plate.

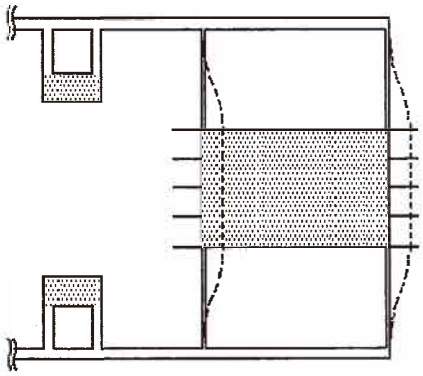

Fig. 4. In-plane motion of the plate.

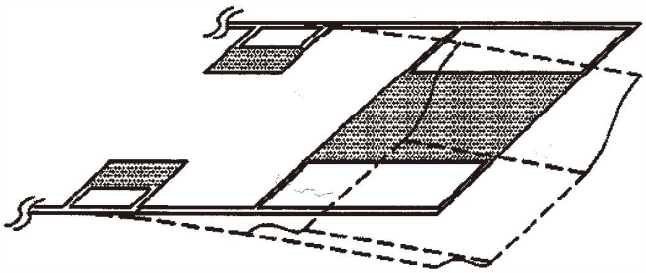

Fig. 5. Out-of-plane motion of the plate.

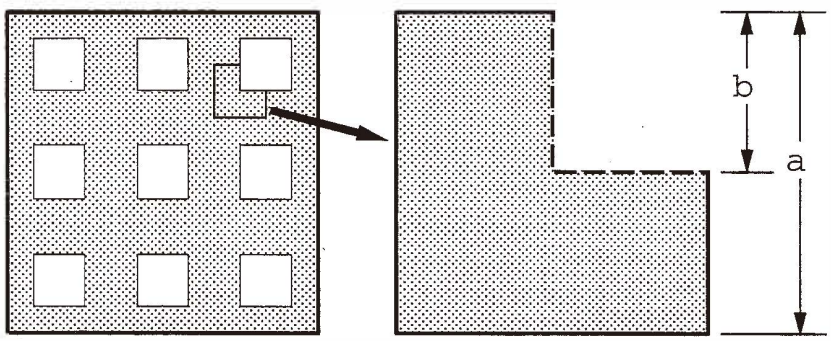

Fig. 6. Squeeze film model for the damping coefficient C_z.

As shown in Fig. 6, only a representative portion of the plate is taken as the problem domain. The underlying assumption is that most of the air escapes through these holes when compressed. The size of the squeeze hole is denoted by b and the size of the domain by a. Boundary conditions are

$$p = 0 \tag{12a}$$

on the sides of the hole and

$$\frac{\partial p}{\partial x} = 0 \text{ or } \frac{\partial p}{\partial y} = 0 \tag{12b}$$

on the rest of the boundary of the domain.

The solution p is calculated using a finite element method with eq. (11) and the boundary conditions in eq. (12). Once the pressure field is obtained, the damping coefficient c_z can be calculated as

$$\begin{aligned} c_z \dot{h} &= \int_{\Omega} p d\Omega \\ &= f_{z,\mathrm{Re}s} \end{aligned} \tag{13}$$

To investigate the effect of hole size on damping, two dimensionless parameters are defined as

$$\alpha = b/a \tag{14}$$

and

$$D_{fac} = f_{z,\mathrm{Re}s} \frac{(h/a)^4}{\mu h \dot{h}} . \tag{15}$$

The value of D_{fac} is calculated and plotted for different values of α and is shown in Fig. 7. When the hole size is known, D_{fac} can be obtained from the plot. Then the damping coefficient can be calculated from the eqs. (13) and (15) as

$$c_z = \mu D_{fac} N \frac{h}{(h/a)^4}, \tag{16}$$

where N is the number of the holes of the plate. The plot in Fig. 7 is very useful for determining the effects of hole size and gap width on the damping coefficient.

The dampings in the x- and z-directions determine the amplitude of the response in the z-direction. The dampings in both directions are functions of the viscosity of air. There-

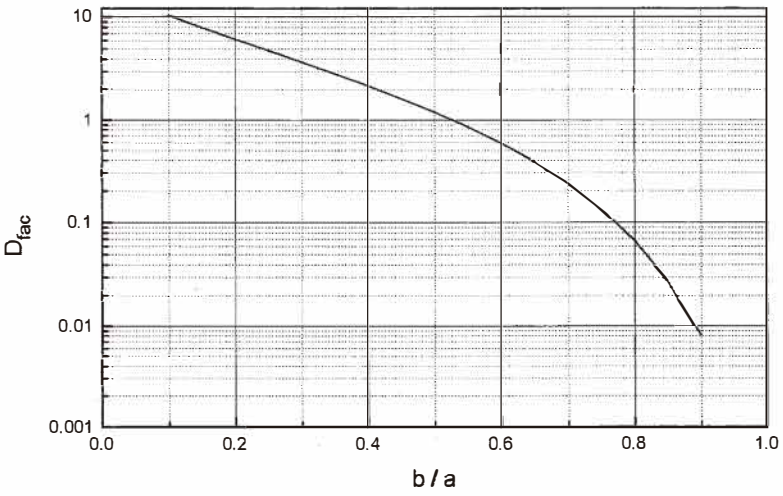

Fig. 7. Dimensionless parameter for the hole size.

fore, the motion in the z-direction in eq. (8) can be explicitly expressed as a function of the air viscosity. The dampings in eqs. (10) and (16) are expressed as constants times the viscosity of air for a fixed hole size.

$$c_x = \mu C_1, \quad C_1 = \frac{A}{h} \tag{17a}$$

$$c_z = \mu C_2, \quad C_2 = D_{fac} N \frac{h}{(h/a)^4} \tag{17b}$$

$$\begin{aligned} R_x &= R_x(c_x) = R_x(\mu) \\ R_z &= R_z(c_z) = R_z(\mu) \end{aligned} \tag{17c}$$

As a result, one can write

$$z = z(R_x, R_z) = E(c_x, c_z) = z(\mu) \ . \tag{18}$$

The actual microgyroscope is driven under very low air pressure. Therefore, once the relation between the viscosity and the air pressure is known, z can be easily predicted using eq. (18).

In fact, as the pressure decreases, the molecular mean path becomes larger, so the rarefied air cannot be treated as a continuum. The air flow under low pressure cannot be considered as a continuum, and is called slip flow. Recently, Veijola *et al.*[5] presented a

model that includes the damping and spring force created by the squeezed air film.

Under low pressure, the flow in a narrow gap can be expressed using the effective viscosity μ_{eff} as

$$\mu_{eff} = \frac{\mu}{1 + f(K_n)}, \tag{19}$$

where μ is the viscosity, $K_n = \lambda/d$ is the Knudsen number, d is the gap width, and λ is the molecular mean free path. The mean free path λ is inversely proportional to pressure[6]

$$\lambda = \frac{P_0}{P}\lambda_0, \tag{20}$$

where P_0 is a reference pressure and λ_0 is the mean free path at pressure P_0. The mean free path λ_0 is 70.0 ± 0.7 nm when the pressure P_0 is 1 atm.

Figure 8 shows the effective viscosity using the function $f(K_n) = 9.683K_n^{1.159}$ presented by Veijola *et al.*[5] Once the relation between viscosity and ambient air pressure is obtained, the output displacement of eq. (18) induced by the external angular velocity can be evaluated for the specified dimensional parameters. To achieve the targeted sensitivity, it is necessary to determine the value of ambient air pressure using the relations discussed above. The sensitivity of the microgyroscope depends on the value of the viscosity of the

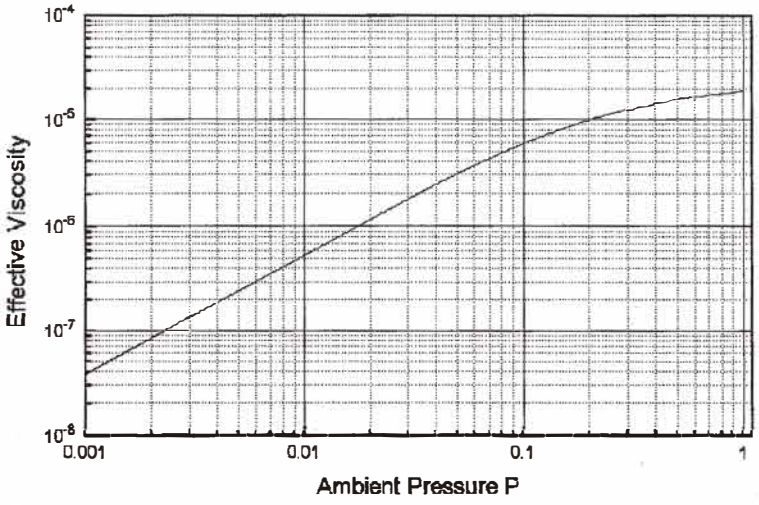

Fig. 8. Effective viscosity coefficient for values of different pressure.

ambient air pressure under which the microgyroscope operates. For the desired specification of this design shown in Table 1, the calculated value of ambient pressure was 0.001 atm.

6. Results and Discussions

Table 1 shows the predicted performance of the microgyroscope using the model discussed. Fabrication errors, however, change the designed dimensions. The effects of fabrication errors can be controlled by the tuning process using the control voltage. In that case, the driving voltage V_D and the pressure also need to be changed to obtain adequate sensitivity to the external angular velocity. Thus, the designed specifications of the microgyroscope deviate from the designed values.

In our fabricated microgyroscopes, the final working frequency has been tuned to 5.8 kHz at a control voltage of 2 V. The driving voltage is increased to an AC drive voltage of 2 V with a DC bias voltage of 3 V at a pressure of 0.00013 atm. The frequency-tuned microgyroscope has been tested on the rate table. Figure 9(a) shows the unmodulated detected signal of 160 $mV_{p\text{-}p}$ under an input angular velocity $\Omega = 0°/s$, and Fig. 9(b) presents the detected output signal of amplitude 20 $mV_{p\text{-}p}$ for $\Omega = 50°/s$ at $f = 4$ Hz. The detected signal in Fig. 9(b) represents an amplitude modulation of the carrier frequency, $f_c = 5.8$ kHz, and the input angular velocity frequency $f = 4$ Hz.

Table 1
Design values of the system variables.

System variables	Designed values
Spring width	3 μm
Thickness	6 μm
Initial gap d_0	2.1 μm
Gap at equilibrium d_{eq}	1.78 μm
Plate mass, m_x	2.43 μg
Effective plate mass in z, m_z	2.57 μg
Stiffness k_x	2.42 M/m
Effective stiffness in z, k_z	3.89 N/m
Working frequency	5.0 kHz
Control voltage V_C	2.3 V
Driving voltage V_D	$1.5 \pm 1.5 \sin\omega t$ V
Sensing range	$\pm$ 180 deg/s
Linearity	1 %FS
Sensitivity C/Ω	$1.2\,fF/$(deg/s)
Working pressure p	0.001 atm

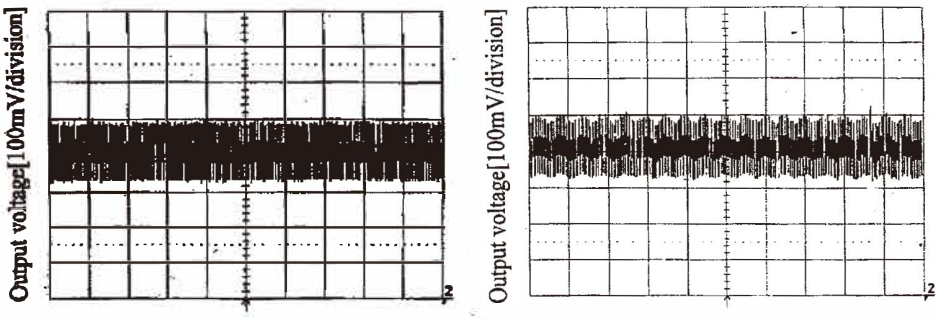

Fig. 9. Output of the frequency-matched microgyroscope (f_c = 5.8 kHz).

7. Conclusion

Dynamic modeling of a surface-machined microgyroscope and practical issues in the modeling have been discussed in detail. In particular, the modeling of dampings was treated in detail. The ideas and procedures presented can be effectively adopted in the design of similar MEMS devices.

The following fundamental questions can be raised. The material properties of Si depend on the fabrication processes, and therefore exact values are unknown in the design stage. Regarding the calculation of damping, several issues must be very carefully treated. The surface roughness of the etched surface of the plate is quite significant compared with other dimensional scales of the structures. Therefore, the validity of the model used in the calculation of dampings should be carefully checked. The working air pressure of the microgyroscope is very low. Therefore, material damping cannot be totally neglected. To clarify these issues, well-designed experimental studies are required.

References

1 J. Bernstein, S. Cho, A. T. King, A. Kourepenis, P. Maciel and M. Weinberg: Proc. IEEE Micro Electro Mechanical Systems Workshops (Ft. Lauderdale 1993) p. 143.
2 K. Tanaka, Y. Mochida, S. Sugimoto, K. Moriya, T. Hasegawa, K. Atsuchi and K. Ohwada: Proc. IEEE Micro Electro Mechanical Systems Workshop (Amsterdam, 1995) p. 278.
3 S. G. Adams, F. M. Bertsch, K. A. Shaw, P. G. Hartwell, N. C. MacDonald and F. C. Moon: Proc. 8th Inter. Conf. Solid-State Sensors and Actuators (Transducers '95) (Stockholm, 1995) p. 438.
4 S. G. Adams, F. M. Bertsch and N. C. MacDonald: Proc. Micro Electro Mechanical Systems Workshop (MEMS '96) (San Diego, 1996) p. 32.
5 T. Veijola, H. Kuisma, J. Lahdenperä and T. Ryhänen: Sensors and Acturators A **48** (1995) 239.
6 S. Dushman: Scientific Foundations of Vacuum Technique (Wiley, New York, 1949).